Mineralogical Magazine, August 2016, Vol. 80(5), pp. 765–780

Adsorption of actinides within speleothems

P. Sengupta[1,*], J. Sanwal[2], N. L. Dudwadkar[3], S. C. Tripathi[3] and P. M. Gandhi[3]

[1] Materials Science Division, Bhabha Atomic Research Centre, Mumbai 400 085, India
[2] Geodynamics Unit, Jawaharlal Nehru Centre for Advanced Scientific Research, Bangalore 560064, India
[3] Fuel Reprocessing Division, Bhabha Atomic Research Centre, Mumbai 400 085, India

[*Received 30 December 2014; Accepted 10 June 2015; Associate Editor: Karen Hudson-Edwards*]

ABSTRACT

Stalagmites and stalactites, as observed within natural caves, may develop inside geological repositories during constructional and post-operational periods. It is therefore important to understand actinide sorption within such materials. Towards this, experimental studies were carried out with ^{233}U, ^{238}Np (VI), ^{238}Np (IV), ^{239}Pu and ^{241}Am radiotracers using natural speleothem samples collected from the Dharamjali cave of the Kumaon Lesser Himalayas, India. Petrological/mineralogical studies showed that natural speleothems have three general domains: (1) columnar calcite; (2) microcrystalline calcite; and (3) botryoidal aragonite – each with ferruginous materials. Results showed that all domains of speleothems can take up >99% actinides, irrespective of valence state and pH (1–6 range) of the solution. However, distribution coefficients were found to be at a maximum in aragonite for most of the actinides. Such data are very important for long-term performance and safety assessments of the deep geological repositories planned for the disposal of high-level nuclear wastes.

Keywords: speleothem, geological repository, nuclear waste disposal, actinides, sorption.

Introduction

Increasing mass awareness on (1) clean energy resources and a secured power supply; and (2) climate change and natural hazards means the importance of nuclear energy within international power programmes is rising steadily. However, public concern over disposal of high-level nuclear wastes, in many cases, has been found to be a growth-limiting factor. It must be understood that for any country with an existing or pre-existing nuclear power program, irrespective of whether it intends to continue or discontinue the same, it is very important to have research and development studies in the field of nuclear waste disposal as there will be waste already in existence that needs to be managed. Needless to say, such academic activities should also be pursued by countries which at present do not have a contribution from nuclear power in their respective 'energy mixture' but aim to have it in the near future.

*E-mail: sengupta@barc.gov.in
DOI: 10.1180/minmag.2016.080.013

Usually, nuclear waste is generated at every stage of an 'open/closed nuclear fuel cycle' and in peaceful applications of radionuclides (Ojovan and Lee, 2005; Sengupta *et al.*, 2013). Extensive studies by previous researchers have identified 'deep geological disposal of high-level nuclear waste' as the safest and most secure management route (Donald, 2010; Ewing, 1999). In brief, irradiation of nuclear fuels (Das *et al.*, 2012; Kutty *et al.*, 2008*a*,*b*; Sengupta *et al.*, 2004, 2013) within reactors generates spent fuels which are kept within air or water-cooled storage facilities for periods of a few months to years. In an 'open fuel cycle', such spent fuels are treated as high-level nuclear waste and therefore merit deep geological disposal (Ojovan and Lee, 2005; Donald, 2010). On the other hand in a 'closed fuel cycle', the spent fuels are further reprocessed to extract valuables, and the concentrated nitric acid stream produced (containing more than 99% of radioactivity witnessed in the cycle) at the end of the process is considered as high-level nuclear waste. This acidic solution contains various radionuclides of ~30–40 different elements, most of which are toxic in nature and emit α-particles or β- and/or γ- rays during its

decay. Due to its hazardous nature over a very long time scale (10^4–10^6 years), the high-level liquid wastes need to be concentrated within an inert matrix and contained in isolation from the biosphere. To achieve this, a 'multiple barrier system' concept is followed which constitutes an 'engineered barrier system' and a 'natural barrier system'. The general practice is to immobilize the high-level liquid waste within borosilicate (Hench *et al.*, 1984; Kaushik *et al.*, 2006; Ojovan and Lee, 2007; Mishra *et al.*, 2007, 2008; Sengupta *et al.*, 2014) and/or phosphate (Kim and Day, 2003; Sengupta, 2012) or aluminosilicate glass (Sengupta *et al.*, 2011*a*) matrices prepared in metallic melter or Joule heated ceramic melter pots (Dutta *et al.*, 2013; Haldar *et al.* 2014; Sengupta, 2011; Sengupta *et al.*, 2006, 2007, 2008, 2009, 2011*b*; Kain *et al.*, 2005). However, laboratory based studies are also being pursued to explore the potential of glass ceramics (Donald *et al.*, 1997; Goswami *et al.*, 2007; Lee *et al.*, 2006; Sharma *et al.*, 2004) and crystalline inert matrices (Haldar *et al.*, 2015; Grover *et al.*, 2006, 2007, 2008, 2010; Jafar *et al.*, 2014*a*,*b*) for this purpose. The immobilized wastes so produced are then put within a stainless steel canister, and two or three such canisters are placed vertically inside another stainless steel container called an overpack. The overpacks are then cooled for a few decades in underground interim storage facilities before they are finally disposed of within a deep geological repository (>300 m) constructed inside suitable host rock formations.

At the initial stage of repository construction, which may extend over few decades, the focus is mainly on drilling boreholes, the excavation of access shafts and laying out galleries and disposal tunnels etc. Such underground excavation procedures involve the use of water for various reasons, which may, ultimately, become localized somewhere within the 'near-field repository environment'. This 'available water' during repository constructions, its operational period and subsequent post-operational stage, together with groundwater/meteoric water can interact with 'cement-based components' of the repository system and the 'excavation damaged/disturbed zones' within repository host rocks. Such water – material interactions can dissolve carbonates and re-precipitate the same in the form of veins, as seen in various geological repository sites such as Forsmark (Sweden; Serrano *et al.*, 2008), Laxemar (Sweden; Gimeno *et al.*, 2014) and Yucca mountain (USA; Quade and Cerling 1990). Also, the formation of speleothems (stalactites: growing down from the roof and stalagmites: building up from the floor), comparable to that seen in caves of karstic terranes, have also been reported from abandoned tunnels, mines etc. (Baker *et al.*, 1999; Boles, 2004; Genty *et al.*, 2001; Kuczumow *et al.*, 2005; Webster *et al.*, 2007) for similar kinds of water–material interaction and re-precipitation processes. One such example is given in Fig. 1 which shows a very initial stage of stalagmite growth within a geological repository. With this in mind, an experimental investigation was carried out in the present study to determine the adsorption of actinides (Ebert *et al.*, 1994; Pirlet, 2001) within naturally occurring speleothems. The term 'adsorption' in the present context adheres strictly to the suggestion of Sposito (1986), i.e. the accumulation of sorbate species at a solution/substrate interface without the development of any three-dimensional networking with the substrate. Thus, 'adsorption' differs from other uptake mechanisms like absorption or surface precipitation or co-precipitation, which either involves structural incorporation of sorbate species within the sorbent (absorption) or the formation of a new phase. To

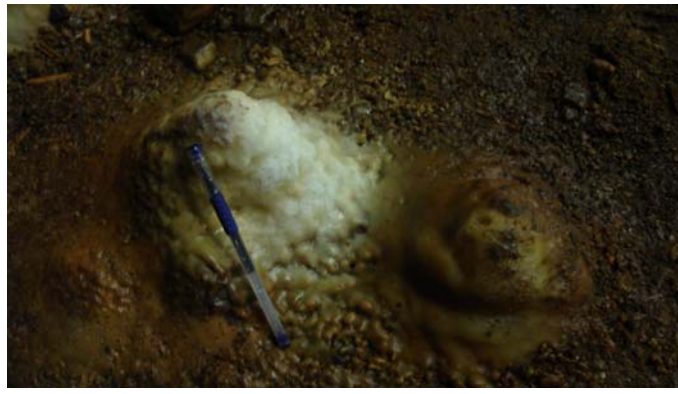

FIG. 1. Growth of a stalagmite within a geological repository.

https://doi.org/10.1180/minmag.2016.080.013 Published online by Cambridge University Press

focus on only the adsorption mechanism, experiments were carried out at a scale of an hour rather than over longer time durations as one or more of the different uptake processes may otherwise come into play. Additionally, to investigate the possibility of long term fluid/sorbate interaction within the geological repository, accelerated experiments were carried out with powdered speleothem domains.

Actinide uptake studies with actual speleothem materials have, to the best knowledge of the authors, not yet been undertaken. Curti (1999) reviewed 'thermodynamic' and 'phenomenological' partition coefficient data available for radionuclides with calcite and identified several gap areas including its (partition coefficient) dependence with solution pH. So far very little work has been done in this regard (Zachara *et al.* 1991; Zavarin *et al.* 2005). Some data are available for calcite and aragonite from pH 6 and upwards but nothing is known in the lower pH range. The present study aims to partially fill this gap, and also develop a new set of actinide adsorption data with natural speleothem material. Note that repository water, if any, will have a pH close to 6–7 or will go slightly up depending on the nature of host rocks, but the acidic environment can only prevail locally due to microbial activity or degradation of synthetic materials like rubber etc. Therefore there is a need to understand the possible radionuclide sorption capabilities of natural carbonates under low-pH conditions.

Experimental

Speleothem sample

Cave environments are known to be extremely complicated in nature due to the simultaneous interplay of a number of factors, such as temperature, partial pressures of carbon dioxide and oxygen, drip-water chemistry, etc. Each of these factors plays a crucial role in the deposition and growth of speleothems within a cave (Fairchild and Baker, 2012). The Dharamjali cave of the Kumaon Lesser Himalayas (India) is also no exception and is known to host a variety of speleothems, some of which are as old as 1800 years (Sanwal *et al.*, 2013). It is evident from the interior/internal geomorphology of the cave that it preserves a wide range of stalagmites (Fig. 2). A 17 cm active stalagmite was collected from this cave (Fig. 3) for the present study. As described in more detail below, the sample is constituted of three different domains, namely translucent, milky-white and grey layers.

For optical microscopic studies, thin slices were prepared from the stalagmite and mounted on transparent glass slides, then ground on different grades of emery papers (until they became transparent to light) and polished with 1 μm fine diamond paste.

Phase analyses

For crystallographic analyses using X-ray diffraction (XRD), powder samples were prepared from all the three different parts of the sample. A microdrill with 0.5 mm core diameter was used to collect small core samples from central domains of relatively coarser material. A BRUKER Discover-8 machine was used to record room temperature XRD patterns from 10–80°2θ. Monochromatized Cu$K\alpha$ radiation (1.54 Å) at 40 kV excitation voltage and 30 mA tube current was employed. For radionuclide sorption studies, same powdered samples from all three domains were used. Using a scanning electron microscope the grain sizes of the powdered

FIG. 2. Interior of Dharamjali cave showing the presence of stalagmites and other common speleothem forms.

https://doi.org/10.1180/minmag.2016.080.013 Published online by Cambridge University Press

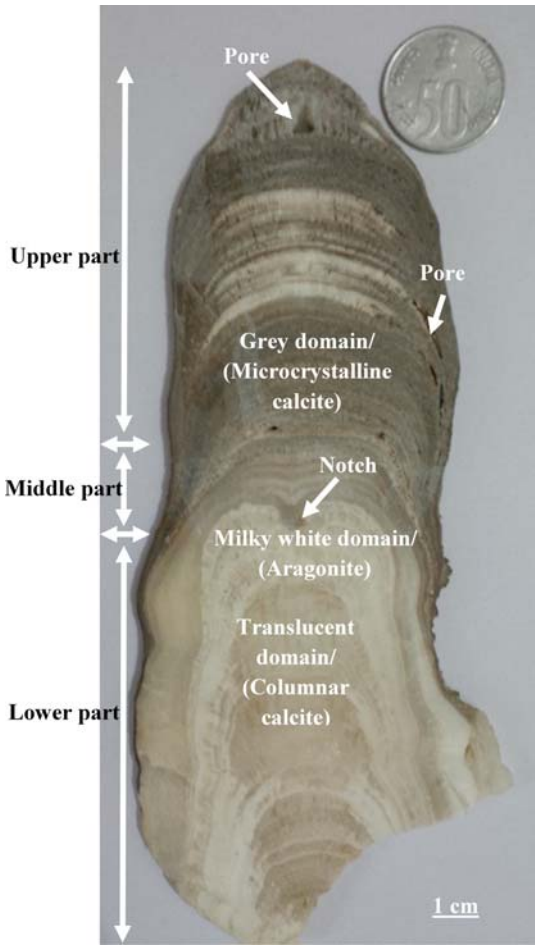

FIG. 3. Cross-section of a stalagmite showing three major layers.

samples were found to vary from 20–50 μm, irrespective of the domains.

Adsorption study

As mentioned earlier, the focus of the present study was the development of a new database on actinide sorption within speleothems as a function of solution pH. Feed solutions spiked with specific radiotracers (^{233}U, ^{238}Np (VI), ^{238}Np (IV), ^{239}Pu and ^{241}Am) in nitric acid medium were used. The radiotracer ^{233}U was separated from streams of a PUREX process[1] and purified by using a cation exchange procedure (Chitnis *et al.*, 1979). The radiotracers ^{238}Np and ^{239}Pu were purified by using an anion exchange method (Ryan and Wheelright, 1959, Mathur *et al.*, 1992) and their respective valence states were maintained through additions of $NaNO_2$ and NH_4VO_3. An americium pure standard solution containing ^{241}Am was used for corresponding sorption studies and the solution was purified following the methods reported by Mathur (1991), Ramanujam *et al.* (1995) and Schulz and Horwitz (1988).

To ensure good quality data, optimization experiments were carried out for sorption kinetics and centrifugation speed, using a powder sample of the milky-white domain and the ^{241}Am radionuclide. The sorption kinetics study (Table 2) was carried out with 0.05 g of milky-white powder at pH = 3 (adjusted with 4% Na_2CO_3 to avoid hydrolysis and polymerization at low pH), for different time intervals (5–60 min), using 5 mL ^{241}Am feed solution (in nitric acid) with a concentration (C_o) of 281.42 mCi/L. Centrifugation speed optimization (Table 3) was undertaken with the same feed solution, keeping the equilibration time constant at 60 min and varying the speed from 2000 to 8000 rpm. Similarly, a volume efficiency study (Table 4) was carried out by varying the feed solution volume from 5–20 mL while keeping the weight of powder (0.05 g), feed solution concentration (^{241}Am: 281.42 mCi/*L*), equilibration time (60 min) and centrifugation speed (8000 rpm) constant. Interference studies (Table 5) have been carried out with multiple elements, e.g. Ca, Na, Ru, Sr and Fe.

Adsorption experiments were performed following a batch equilibration route where extractions were carried out with a vortex shaker for the fixed interval of 60 min. A fixed amount of powdered samples (0.05 g) were added to 5 mL distilled water spiked separately with ^{233}U, ^{238}Np (VI), ^{238}Np (IV), ^{239}Pu and ^{241}Am containing nitric acid feed solution, maintained at a fixed pH, ranging from 1 to 6. Concentrated HNO_3 and 4% Na_2CO_3 were used to adjust pH values of the solutions. The samples were equilibrated over a fixed interval of 60 min at room temperature. For all radiotracers, separate examinations with blank solutions were carried out to verify wall absorption of the extraction vials and were found to be negligible. For estimation, after 60 min the solution was filtered and 0.02 mL of solution was plancheted and counted. A ZnS(Ag) alpha scintillation counter calibrated against standard ^{239}Pu was used for

[1]Plutonium Uranium Redox EXtraction, a process for the reprocessing of spent nuclear fuel to separate uranium and plutonium from the fission products and from one another.

https://doi.org/10.1180/minmag.2016.080.013 Published online by Cambridge University Press

TABLE 1. Speleothem phases.

Speleothem domains (phase)	Lattice parameters [Å]			Unit-cell volume [Å^3]
	a	*b*	*c*	
Translucent (Columnar calcite)	4.991 ± 0.012	4.991 ± 0.012	17.006 ± 0.026	366.86 ± 1.068
Calcite (JCPDS 81-2027)	4.991	4.991	17.06	368.07
Milky white (aragonite)	4.975 ± 0.012	7.965 ± 0.011	5.702 ± 0.009	225.98 ± 0.72
Grey (aragonite + calcite)	4.950 ± 0.013	7.947 ± 0.016	5.730 ± 0.009	225.47 ± 0.82
Aragonite (JCPDS 76-0606)	4.959	7.964	5.737	226.65

TABLE 2. Sorption kinetics of ^{241}Am using a powdered aragonite domain (M = 0.05 g) and ^{241}Am feed solution*.

Equilibration time (min)	Effluent concentration (mCi/L) C_e	Decontamination factor (C_o/C_e)	% Sorption	K_d (mL/g)
5	221.45	1.27	28.42	39.69
15	171.40	1.64	50.11	100.44
30	84.94	3.31	77.28	340.13
60	1.003	280.77	99.64	27,958

*Concentration (C_o) = 281.42 mCi/L; pH 3; equilibration time: 60 min).
% Sorption = $(C_o - C_e) \times 100/C_o$, $K_d = (C_o - C_e) \times V/(C_e \times M)$, see text for details.

TABLE 3. Optimization of centrifugation speed using a powdered aragonite domain (M = 0.05 g) and ^{241}Am feed solution*.

Rotational speed (rpm)	Effluent concentration (mCi/L) C_e	% Sorption	K_d (mL/g)
2000	4.05	98.56	6849
3000	3.94	98.60	7043
5000	1.003	99.64	27,958
7000	0.817	99.70	34,346
8000	0.816	99.71	34,388

*Concentration (C_o) = 281.42 mCi/L; pH 3; equilibration time: 60 min.
% Sorption = $(C_o - C_e) \times 100/C_o$, $K_d = (C_o - C_e) \times V/(C_e \times M)$, see text for details.

^{233}U and ^{239}Pu. For all other isotopes, a single channel gamma analyser with NaI(Tl) detector was used.

The distribution coefficient (K_d), was calculated by the following equation:

$$K_d = V(C_o - C_e)/(C_e \times M) \quad (1)$$

where C_o and C_e are feed and effluent concentrations, respectively; V is volume (mL) of solution and M is the amount of ion exchanger/adsorbent used.

Results

A full length cross-section image of the stalagmite collected, measuring ~17 cm, is shown in Fig. 3. Broadly, the sample consisted of translucent, milky-white and grey layers. The lower portion of the sample was made up of milky-white and translucent layers, in which the thickness varied widely (from a few hundred micrometres to tens of millimetres). The central portion of the lower part was constituted dominantly of thicker translucent layers intercalated with very thin milky white

https://doi.org/10.1180/minmag.2016.080.013 Published online by Cambridge University Press

TABLE 4. Volume efficiency studies using a powdered aragonite domain ($M = 0.05$ g) and ^{241}Am feed solution*.

Feed solution volume (mL)	Effluent concentration (mCi/L), C_e	% Sorption	Decontamination factor (C_o/ C_e)	K_d (mL/g)
5	1.003	99.64	280.77	27958
10	3.2145	98.86	87.66	17389
20	7.4632	97.35	37.72	14690

*Concentration (C_o) = 281.42 mCi/L; pH 3; equilibration time: 60 min.
% Sorption = $(C_o - C_e) \times 100/C_o$, $K_d = (C_o - C_e) \times V/(C_e \times M)$, see text for details.

TABLE 5. Interference studies using a powdered aragonite domain ($M = 0.05$ g) and ^{241}Am feed solution.*

Interfering element at pH 3	Concentration of interfering element, (g/L)	Effluent concentration (mCi/L), C_e	% Sorption	K_d (mL/g)
Ca	1	2.710	99.04	27871
Ca	5	10.2	96.38	2659
Ca	10	20.1	92.85	1300
Na	1	5.5	98.05	6154
Na	5	14.64	96.23	1885
Na	10	24.22	91.39	1215
Ru	0.1	2.8	99.0	9951
Ru	0.5	9.47	96.63	2872
Ru	1	17.54	93.77	1502
Sr	1	6.98	97.52	3932
Sr	5	18.46	93.44	1425
Sr	10	30.92	89.01	811
Fe	1	8.32	97.04	3282
Fe	5	21.84	92.24	1189
Fe	10	35.42	87.41	694

*Concentration (C_o) = 281.42 mCi/L; pH 3; equilibration time: 60 min.
% Sorption = $(C_o - C_e) \times 100/C_o$, $K_d = (C_o - C_e) \times V/(C_e \times M)$, see text for details.

layers along the growth axis. However at the limb sides, an accumulation of milky-white layers followed by greyish-white layers was observed. At the top of the lower part, a notch was present within the milky-white layer. Above the notch alternate intercalations of very thin milky-white/ greyish-white layers, draping the notch completely, were observed. Note that both the middle and lower parts of the stalagmite were free from pores, which was not the case for the upper part, dominated by grey layers. The fraction of the milky-white layer was found to be reduced drastically within the upper part.

Optical micrographs of translucent, grey and milky-white layers are given in Figs 4*a–c*. It is noted that translucent (Fig. 4*a*) and milky-white layers (Fig. 4*c*) are constituted of coarse columnar calcites and botryoidal-type (fan-like fabric radiating from a central nucleus) aragonite, respectively, whereas grey layers, though constituted dominantly of interlayered fine-grained microcrystalline calcite and unidentified brownish/greyish phase(s) (Fig. 4*b*), also contained small amounts of aragonite. This is further confirmed by X-ray diffraction data (Fig. 5) in which peak-positions have been identified using the database of the

https://doi.org/10.1180/minmag.2016.080.013 Published online by Cambridge University Press

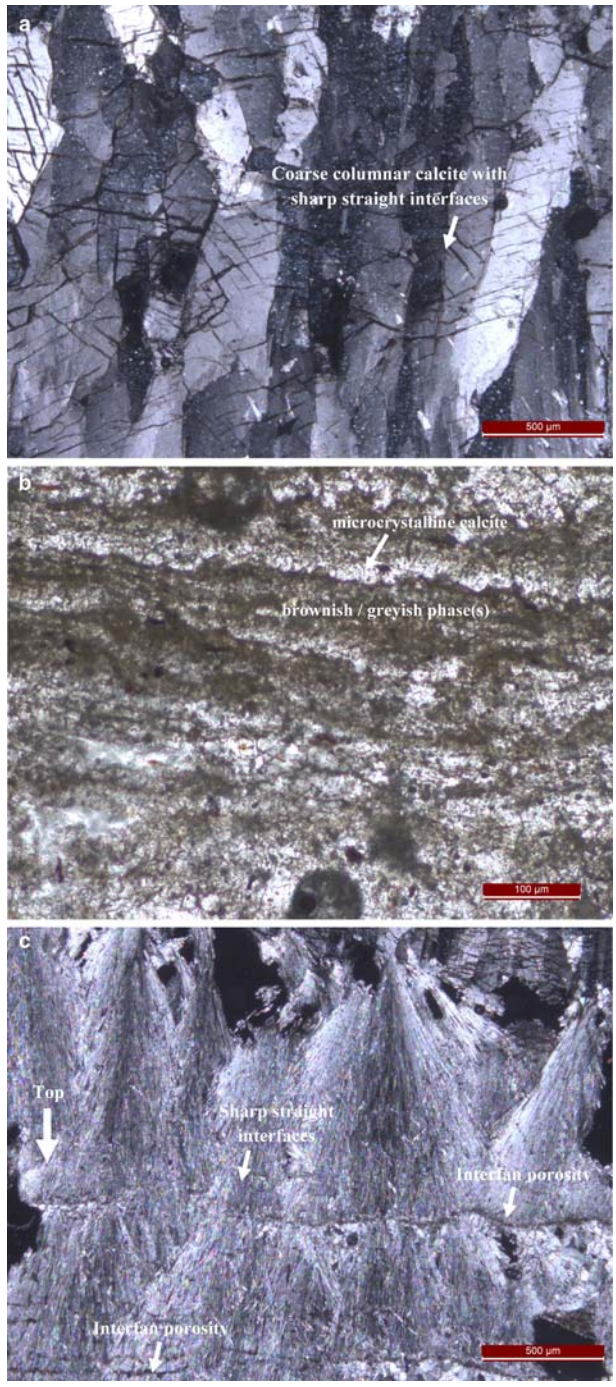

FIG. 4. Crossed-polar optical images showing the presence of (*a*) coarse columnar calcite crystals within a translucent layer; (*b*) microcrystalline calcite interlayered with unidentified brownish/greyish phase(s) within grey layers; and (*c*) botryoidal fibrous aragonite crystals that define the milky-white layers. Interfan porosity increases towards the top, giving rise to the appearance of growth banding patterns.

https://doi.org/10.1180/minmag.2016.080.013 Published online by Cambridge University Press

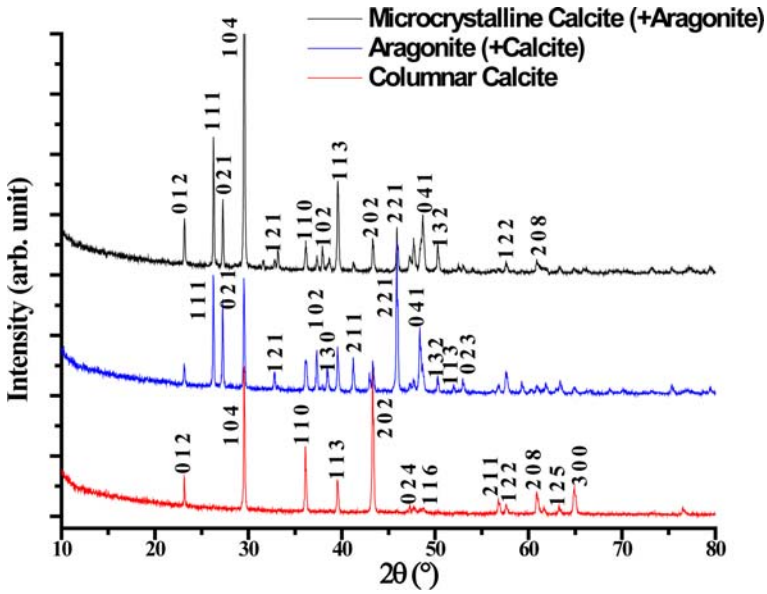

FIG. 5. X-ray diffraction patterns obtained from the different domains of the speleothem.

International Centre of Diffraction Data (JCPDS-ICDD). Lattice parameters for different domains have also been measured and compared with the standard database (Table 1). The micrographs of columnar calcite grains identify them as 'palisadic type' i.e. grains with straight parallel sides having a long axis coinciding with direction of growth. Aragonite crystals are found to be mostly acicular (with needle-like terminations), but the presence of a few ray-type varieties (with square-like terminations) is also noted. It is apparent from optical images that layers constituted of coarse columnar calcites and botryoidal aragonite are massive in nature whereas the microcrystalline calcite-bearing domains show a very fine interlayered structure. Interfacial contacts between columnar calcite crystals and aragonite crystals are found to be sharp and straight whereas those of microcrystalline calcites are very irregular. Within the aragonite domains interfan porosities are noted which has imparted a discontinuous banding structure. The presence of detrital matters was seen in all domains.

Detail experimental results for sorption studies are given in Tables 5–10. For all five radionuclides, sorption coefficients within powdered aragonite, columnar calcite and microcrystalline calcite domains are found to be >99%. In each case distribution coefficients are found to increase with increasing pH (Figs 6*a–e*). Such a sympathetic relationship can be explained by the speciation change model of van Cappellen *et al.* (1993) who showed that at high pH, a carbonate surface becomes dominated by $>CO_3^-$ terminations while at low pH it is dominated by $>Ca^{2+}$ or $>CaOH_2^+$ terminations. Therefore, a rise in solution pH facilitates adsorption of actinide cations (e.g. Np $(V)O_2^+$) on a carbonate surface.

Overall, ^{233}U and $^{238}Np(VI)$ exhibited large amounts of sorption on speleothem materials while ^{239}Pu and $^{238}Np(IV)$ showed the least (Tables 6–10). A comparison of K_d values for ^{238}Np (VI) (Table 9) with ^{238}Np (IV) (Table 10) clearly indicates that radionuclides at higher valence states get more adsorped on speleothem materials. Interestingly the trend in K_d values for ^{238}Np (VI) (Table 9, Fig. 6*d*) within aragonite, columnar calcite and microcrystalline calcite has been reversed from low pH (aragonite > columnar calcite > microcrystalline calcite) to higher pH (aragonite < columnar calcite < microcrystalline calcite). For the case of ^{238}Np (IV) (Table 10, Fig. 6*e*) the K_d variation trend within the speleothem materials remained unaltered (aragonite > microcrystalline calcite > columnar calcite) with pH variation. Earlier Keeney-Kennicutt *et al.* (1984) noted that at pH 8 in distilled water, aragonite has a greater tendency to adsorb $^{238}Np(V)$ than calcite, although the measured K_d values were less by few orders compared to present values. Such variations however could be due to differences in: (1) surface area and compositions of

https://doi.org/10.1180/minmag.2016.080.013 Published online by Cambridge University Press

TABLE 6. Sorption studies using ^{241}Am* on 0.05 g (=M) powdered aragonite, columnar calcite and microcrystalline calcite domains over a pH range of 1–6.

pH	Effluent concentration (μCi/L) C_e			% Sorption			Decontamination factor (C_0/ C_e)			K_d (mL/g)		
	Δ	○	□	Δ	○	□	Δ	○	□	Δ	○	□
1	1446.18	1146.13	1012.18	99.48	99.82	99.64	194.60	245.57	278.08	19,359	24,371	27,763
2	1290.22	1090.42	990.22	99.54	99.77	99.65	218.12	258.18	284.26	21,715	25,718	28,326
3	1003.70	903.70	903.70	99.64	99.75	99.68	281.41	311.31	311.31	27,938	31,065	31,169
4	936.55	736.55	853.55	99.66	99.59	99.69	300.25	381.85	329.53	29,966	38,085	32,853
5	743.58	743.55	823.58	99.74	99.70	99.70	378.46	378.25	341.53	37,746	37,725	34,094
6	712.44	612.41	660.44	99.75	99.69	99.76	395.00	459.84	426.39	39,400	45,884	42,539

*5 mL of feed solution with initial concentration, C_o = 281.42 mCi/L; equilibration time: 60 min with vortex shaker.
% Sorption = $(C_o - C_e) \times 100/C_o$, $K_d = (C_o - C_e) \times V/(C_e \times M)$, see text for details.
Δ aragonite, ○ columnar calcite, □ microcrystalline calcite domains.

TABLE 7. Sorption studies using ^{233}U* on 0.05 g (=M) powdered aragonite, columnar calcite and microcrystalline calcite domains over a pH range of 1–6.

pH	Effluent concentration (μCi/L) C_e			% Sorption			Decontamination factor (C_0/ C_e)			K_d (mL/g)		
	Δ	○	□	Δ	○	□	Δ	○	□	Δ	○	□
1	300.40	240.40	425.98	99.92	99.94	99.90	1413.00	1767.16	995.54	141,273	1766.17	99,458
2	260.34	230.14	369.34	99.93	99.95	99.91	1629.10	1844.00	1159.38	162,810	184,300	114,838
3	240.82	219.82	320.83	99.94	99.95	99.92	1761.15	1945.50	1325.37	176,014	192,682	131,987
4	203.44	136.42	298.24	99.95	99.97	99.93	2089.26	3118.50	1423.22	208,374	311,752	142,222
5	180.66	110.66	230.66	99.96	99.97	99.94	2347.61	3855.36	1844.00	234,661	385,464	183,502
6	140.26	98.86	210.41	99.97	99.98	99.95	3023.81	4327.75	2019.62	302,281	432,676	201,862

*5 mL of feed solution with initial concentration, C_o = 424.12 mCi/L; equilibration time: 60 min with vortex shaker.
% Sorption = $(C_o - C_e) \times 100/C_o$, $K_d = (C_o - C_e) \times V/(C_e \times M)$, see text for details.
Δ aragonite, ○ columnar calcite, □ microcrystalline calcite domains.

TABLE 8. Sorption studies using ^{239}Pu* on 0.05 g (=M) powdered aragonite, columnar calcite and microcrystalline calcite domains over a pH range of 1–6.

pH	Effluent concentration (μCi/L) C_e			% Sorption			Decontamination factor (C_0/ C_e)			K_d (mL/g)		
	Δ	○	□	Δ	○	□	Δ	○	□	Δ	○	□
1	2290.02	1990.00	3245.43	99.45	99.52	99.22	182.93	210.51	128.90	18,193	20,950	12,837
2	1940.00	1710.00	2987.09	99.54	99.59	99.28	215.93	244.98	140.10	21,493	24,398	13,910
3	1869.14	1689.10	2783.32	99.55	99.60	99.34	224.14	247.88	150.69	22,313	24,688	14,969
4	1550.18	1450.18	2673.44	99.63	99.65	99.40	217.26	288.90	156.90	26,926	28,790	15,590
5	1334.52	1234.55	2532.56	99.68	99.71	99.68	314.00	340.58	165.58	31,302	33,958	16,458
6	1226.34	1006.33	2502.73	99.71	99.76	99.70	341.69	417.90	167.56	34,068	41,791	16,656

*5 mL of feed solution with initial concentration, C_o = 418.91 mCi/L; equilibration time: 60 min with vortex shaker.
% Sorption = $(C_o - C_e) \times 100/C_o$, $K_d = (C_o - C_e) \times V/(C_e \times M)$, see text for details.
Δ aragonite, ○ columnar calcite, □ microcrystalline calcite domains.

https://doi.org/10.1180/minmag.2016.080.013 Published online by Cambridge University Press

TABLE 9. Sorption studies using ^{238}Np(VI)* on 0.05 g (=*M*) powdered aragonite, columnar calcite and microcrystalline calcite domains over a pH range of 1–6.

pH	Effluent concentration (μCi/L) C_e			% Sorption			Decontamination factor (C_0/ C_e)			K_d (mL/g)		
	Δ	◯	□	Δ	◯	□	Δ	◯	□	Δ	◯	□
1	340.42	440.49	490.49	99.92	99.90	99.89	401.00	988.64	888.75	127,841	98,763	88,676
2	279.14	310.44	306.44	99.93	99.93	99.93	1559.14	1401.24	1421.56	155,813	140,222	144,900
3	256.60	296.90	210.90	99.94	99.93	99.95	1576.10	1464.65	2061.61	169,821	146,364	207,043
4	224.24	210.74	202.74	99.95	99.95	99.95	1941.96	2071.43	2142.85	194,996	194,996	217,400
5	198.64	160.60	134.60	99.95	99.96	99.97	2196.96	2718.75	3245.26	219,596	207,043	207,043
6	165.36	113.65	90.65	99.96	99.97	99.98	2636.36	3849.55	4833.33	263,536	384,855	483,233

*5 mL of feed solution with initial concentration, C_o = 435 mCi/L; equilibration time: 60 min with vortex shaker.
% Sorption = $(C_o - C_e) \times 100/C_o$, $K_d = (C_o - C_e) \times V/(C_e \times M)$.
Δ aragonite, ◯ columnar calcite, □ microcrystalline calcite domains.

TABLE 10. Sorption studies using ^{238}Np(IV)* on 0.05 g (=*M*) powdered aragonite, columnar calcite and microcrystalline calcite domains over a pH range of 1–6.

pH	Effluent concentration (μCi/L) C_e			% Sorption			Decontamination factor (C_0/ C_e)			K_d (mL/g)		
	Δ	◯	□	Δ	◯	□	Δ	◯	□	Δ	◯	□
1	2380.01	1980.01	2176.01	99.45	99.53	99.49	178.57	214.65	195.31	17,757	21,364	19,395
2	1990.06	1543.06	1843.26	99.53	99.64	99.57	213.56	275.97	230.60	21,257	27,442	22,998
3	1888.12	1452.12	1652.18	99.55	99.66	99.61	226.10	292.70	257.58	22,387	29,167	25,658
4	1598.14	1294.14	1495.24	99.56	99.70	99.65	265.63	328.44	283.33	26,496	32,740	28,423
5	1421.59	1129.59	1221.50	99.67	99.73	99.71	299.30	379.44	348.36	29,830	37,524	34,736
6	1373.38	1100.38	1167.31	99.68	99.74	99.72	309.54	386.37	363.25	30,854	38,523	36,225

*5 mL of feed solution with initial concentration, C_o = 425 mCi/L; equilibration time: 60 min with vortex shaker.
% Sorption = $(C_o - C_e) \times 100/C_o$, $K_d = (C_o - C_e) \times V/(C_e \times M)$.
Δ aragonite, ◯ columnar calcite, □ microcrystalline calcite domains.

calcite powder used; (2) ^{238}Np valence state; (3) concentration of ^{238}Np within solution; (4) solution compositions; and (5) any combination of such factors.

Sorption of ^{239}Pu on speleothem materials also showed a positive correlation with pH, and the K_d variation trend remained the same throughout i.e. columnar calcite > aragonite > microcrystalline calcite. In a separate study Zavarin *et al.* (2005) reported that the sorption of Pu(IV) to calcite was higher than Pu(V) over the entire examined pH range and the K_d values decreased both at low and high pHs.

Like ^{239}Pu, ^{233}U also exhibited a rise in actinide sorption with pH and maintained a similar K_d variation trend i.e. columnar calcite > aragonite > microcrystalline calcite. However, Carroll and Bruno (1991) reported a weak correlation between the sorption of U(VI) to calcite and pH variation.

In the case of ^{241}Am, higher K_d values were obtained for columnar calcite in comparison to aragonite throughout the pH range. Shanbhag and Morse (1982) measured Am(III) sorption on calcite in seawater and found K_d values greater than 10^5 mL/g.

Discussion

Speleothem mineralogy and texture are essentially controlled by changes in: (1) solute/substrate interface conditions; and/or (2) supply of constituents; (3) the pressure–temperature–fugacity of CO_2

https://doi.org/10.1180/minmag.2016.080.013 Published online by Cambridge University Press

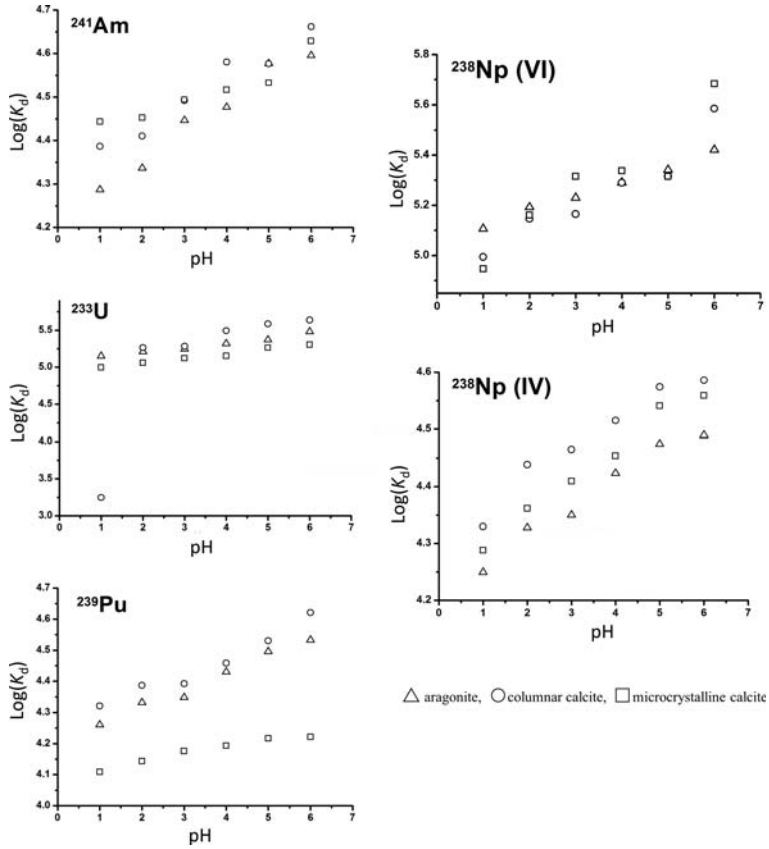

FIG. 6. Variation of log(K_d) of ^{233}U, ^{241}Am, ^{239}Pu and ^{238}Np present in different phases of the speleothem and $CaCO_3$ minerals from the literature as a function of pH.

system within cave; (4) dripping water chemistry and flow rate; and (5) phase stability fields etc. (Given and Wilkinson, 1985; Burton and Walter, 1987; White, 1997; Fairchild and Baker, 2012). Wide variation in crystal morphology is essentially linked to nucleation and dominant growth mechanisms. For example according to Broughton (1983), the observed features of grey layers i.e. microcrystalline calcite and its interlamellar nature, could be due to the presence of a thin (<100 μm) film solution on the speolothem surface. Observed random orientations of microcrystals, irregular (serrated to intercalated) grain boundaries and patchy extinction are all suggestive of an extremely disturbed growth environment with fluctuations in water flow rate and nutrient supply. An interlamellar texture possibly implies that such fluctuations were repetitive in nature. On the other hand, the observed botryoidal texture of the milky-white layer domains is indicative of a crystallite coalescence growth mechanism, leading to competitive growth fabrics. Contrary to this, the columnar fabric of translucent layer domains is indicative of unperturbed crystal growth mechanisms under continuous constituent ion (e.g. Ca^{2+}, CO_3^{2-}) supply conditions facilitated by a higher cave-water drip rate (Genty and Quinif, 1996). This is further substantiated by sharp straight crystalline outlines and uniform extinction. From detailed petrological and geochemical studies, Railsback *et al.* (1994) concluded that for the speleothem of Drotsky's cave (Botswana) calcite layers were precipitated in the wet season whereas aragonite layers were deposited in the dry season. The absence of any textural evidence suggestive of a generation of columnar calcite through diagenetic alteration (recrystallization) of botryoidal aragonite, such as (1) columnar calcite crystals replacing botryoidal aragonite and (2) occurrence or relics of aragonite within columnar calcite, clearly indicates its (columnar calcite) primary nature.

https://doi.org/10.1180/minmag.2016.080.013 Published online by Cambridge University Press

Radionuclide adsorption studies using ^{233}U, $^{238}Np(VI)$, $^{238}Np(IV)$, ^{239}Pu and ^{241}Am with powdered columnar calcite, microcrystalline calcite and botryoidal aragonite, over a solution pH range of 1–6, showed sorption capacities greater than 99%. This means within a geological repository set up, in addition to an engineered barrier system, speleothem structures can also act as barrier to actinide migration. It should be emphasized here that due caution should be exercised while comparing the present data with those obtained from polycrystalline aggregates of pure calcite or aragonite. For example, in general, the dissolution of calcite is expected under an acidic environment whereas in the present case a substantial amount of solid mass was always found to be present at the end of the sorption experiments. This anomaly may be due to improvement in the chemical durability of speleothem carbonates through impurity diffusion in their corresponding lattices and/or may be an accumulation of impurities at the end of the experiments. Optical images given in Fig. 4 show clearly the presence of impurities in various speleothem domains.

A comparison of measured K_d values for powdered columnar calcite, microcrystalline calcite and botryoidal aragonite shows the later has the maximum capability to hold actinides on its surface. Crystal structure and chemistry play a dominant role in the sorption of actinides on carbonate minerals (Sturchio *et al.*, 1998; Reeder *et al.*, 2000, 2001; Kelly *et al.*, 2003, 2006). For example, the uranyl ion, which has a linear uranyl moiety $(O=U=O)^{2+}$ (Russell *et al.*, 1994) is known to prefer aragonite over calcite, probably due to its structural similarity (orthorhombic) with rutherfordine [$UO_2(CO_3)$, Christ *et al.*, 1955)]. In fact, the solid solution distribution coefficient of the uranyl ion in aragonite has been found to be an order higher in comparison to calcite (Russell *et al.*, 1994; Kelly *et al.*, 2003). Stumpf and Franghänel (2002) studied the mode of interaction between trivalent actinide and calcite using Time Resolved Laser Fluorescence Spectroscopy (TRLFS). They considered the curium (Cm(III)) ion as representative for trivalent actinides and reported a two-step process. In the first step, each Cm(III) substituted for Ca(II) ions present on the surface of calcite and became linked to six oxygen ions from the carbonate anions of the calcite lattice; two oxygen ions of the surface bonded carbonate anion belonging to the aqueous medium; and one water molecule. Therefore, Ca(II) ions in 6-fold coordination within calcite were replaced by Cm(III) ions in 9-fold coordination. With time (on a scale of months), the surficial Cm(III) was dehydrated and became part of calcite lattice. Therefore the coordination number of Cm(III) was reduced from an initial 9 to 6. Such an exchange mechanism is expected to change significantly in aragonite as Ca(II) occurs in 9-fold coordination within it instead of 6-fold (Deer *et al.* 1992). This probably explains the observed higher K_d values for botryoidal aragonite than microcrystalline calcite, in most of the cases. In fact, a similar argument was extended earlier to justify greater inclusion of the uranyl cation (UO_2^{2+}) within aragonite than in calcite (Kitano and Oomori, 1971; Meece and Benninger, 1993; Railsback, 1999). It therefore appears that it will be prudent to stabilize aragonite as much as possible within a geological repository system so as to ensure better environmental safety.

This is a very important observation from a geological repository safety assessment view, as it indicates that in unprecedented events of 'engineered barrier system failures', speleothems can arrest the migration of actinides significantly within the 'near-field' region. Further, among the different domains of speleothems, it is noted that botryoidal aragonite offers the highest K_d values for the actinides, irrespective of its valence state and the pH of the adjacent solution. It is therefore suggested that efforts should be taken towards greater stabilization of aragonite within deep geological repository systems. Further, the measured K_d values can be used to develop a consistent database of parameters for modelling of radionuclide migrations within geological repositories.

Summary

Sorption is a key process responsible for the retardation of radionuclide transport in a natural environment. A review on internal morphological evolution of abandoned tunnels, mines etc. shows the possibility of speleothem formation, much in the same way as witnessed in natural caves. Therefore it is very important to assess the role of such speleothem materials on the migration of radionuclides within a geological repository, during operation and post-operational phases. So far no attention has been given to this area. To fill this gap the present experimental study was carried out using natural speleothem material obtained from the Dharamjali cave of the eastern Kumaun Himalaya.

Optical microscopy and X-ray diffraction analyses identified the presence of three domains, namely translucent, milky-white and grey layers,

https://doi.org/10.1180/minmag.2016.080.013 Published online by Cambridge University Press

constituted dominantly of columnar calcite, botryoidal aragonite and microcrystalline calcite (with some unidentified ferruginous material), respectively. Systematic adsorption studies with powdered speleothem components (accelerated scenario), using ^{233}U, ^{238}Np (VI), ^{238}Np (IV), ^{239}Pu and ^{241}Am radiotracers over a pH range of 1–6, have been carried out in the present investigation. On the whole it is noted that all speleothem components exhibit sorption capacities >99%. This means that speleothems can arrest or restrict actinide migrations within the 'near-field' region of a geological repository. Among the different speleothem phases, botryoidal aragonite exhibits the highest K_d values for the actinides, irrespective of its valence state and the pH of the adjacent solution. It is therefore apparent that stabilization of aragonite within a repository environment will be beneficial for its isolation from the biosphere. Further, the measured K_d values can be used to develop a consistent database of parameters for modelling of radionuclide migrations within geological repositories.

Finally we emphasize that understanding or predicting actinide sorption mechanism(s) at mineral-fluid interfaces at different microscopic length scales, and its implications on field scales under continuously evolving repository environments over a long time scale is an extremely difficult task and therefore merits a modelling approach. The present laboratory-based experimental data is a small quantitative contribution towards such an integrated multidisciplinary initiative.

Acknowledgements

The authors are grateful to Dr. G.K. Dey, Associate Director, Materials Group, BARC and Prof. K.S. Valdiya and Prof. C.P. Rajendran of JNCASR, Bangalore for their encouragements in the study. JS acknowledges the financial support received from DST SERC Fast Track Scheme (No. SR/FTP/ES-97/2009).

References

Baker, A., Mockler, N.J., Barnes, W.L. (1999) Fluorescence intensity variations of speleothem-forming goundwaters: implications for palaeoclime reconstruction. *Water Resources Research*, **35**, 407–413.

Boles, J.R. (2004) Rapid growth of meter scale calcite speleothems in Mission Tunnel, Santa Brbara, CA. Pp. 353–356 in: *Water-Rock Interaction* (R.B. Wanty and R.R. SealII, editors). Taylor and Francis Group, London.

Broughton, P.L. (1983) Environmental implications of competitive growth fabrics in stalactic carbonate. *International Journal of Speleology*, **13**, 31–41.

Burton, E.A. and Walter, L.M. (1987) Relative precipitation rates of aragonite and Mg calcite from seawater: temperature or carbonate ion control. *Geology*, **15**, 111–114.

Carroll, S.A. and Bruno, J. (1991) Mineral-solution interactions in the U(VI)–CO_2–H_2O system. *Radiochimica Acta*, **52–53**, 187–193.

Chitnis, R.T., Rajappan, S.V., Kumar, S.V. and Nadkarni, M.N. (1979) *Cation exchange separation of uranium and thorium*. Report BARC-1003, Bhabha Atomic Research Centre, Mumbai.

Christ, C.L., Clark, J.R. and Evans, H.T. (1955) Crystal structure of rutherfordine, UO_2CO_3. *Science*, **121**, 472–473.

Curti, E. (1999) Coprecipitation of radionuclides with calcite: estimation of partition coefficients based on a review of laboratory investigations and geochemical data. *Applied Geochemistry*, **14**, 433–445.

Das, N., Sengupta, P., Roychowdhury, S., Sharma, G., Gawde, P.S., Arya, A., Kain, V., Kulkarni, U.D., Chakravartty, J.K. and Dey, G.K. (2012) Metallurgical characterizations of Fe-Cr-Ni-Zr base alloys developed for geological disposal of radioactive hulls. *Journal of Nuclear Materials*, **420**, 559–574.

Deer, W.A., Howie, R.A. and Zussman, J. (1992) *An Introduction to the Rock Forming Minerals.* John Wiley and Sons Inc, New York.

Donald, I.W. (2010) *Waste Immobilization in Glass and Ceramic Based Hosts.* Wiley and Sons, 493 Pp.

Donald, I.W., Metcalfe, B.L. and Taylor, J.R.N. (1997) Review: the immobilization of high level radioactive wastes using ceramics and glasses. *Journal of Material Science*, **32**, 851–887.

Dutta, R.S., Yusufali, C., Paul, B., Majumdar, S., Sengupta, P., Mishra, R.K., Kaushik, C.P., Kshirsagar, R.J., Kulkarni, U.D. and Dey, G.K. (2013) Formation of diffusion barrier coating on superalloy 690 substrate and its stability in borosilicate melt at elevated temperature. *Journal of Nuclear Materials*, **432**, 72–77.

Ebert, W.L., Bates, J.K., Buck, E.C., Gong, M. and Wolf, S. F. (1994) Disposition of actinides released from high level waste glass. *Proceedings of the American Ceramic Society 96th Annual Meeting*, Indianapolis, USA.

Ewing, R.C. (1999) Radioactivity and the 20th Century. Pp. 1–22 in: *Uranium: Mineralogy, Geochemistry and the Environment* (P.C. Burns and R.J. Finch, editors). Reviews in Mineralogy, **38**. Mineralogical Society of America, Washington DC.

Fairchild, I.J. and Baker, A. (2012) *Speleothem Science: From Process to Past Environments.* Wiley–Blackwell, 450 Pp.

Genty, D. and Quinif, Y. (1996) Annually laminated sequences in the internal structure of some Belgian

https://doi.org/10.1180/minmag.2016.080.013 Published online by Cambridge University Press

stalagmites – Importance for paleoclimatology. *Journal of Sedimentary Research*, **66**, 275–288.

Genty, D., Baker, A. and Vokal, B. (2001) Intra- and inter-annual growth rate of modern stalagmites. *Chemical Geology*, **176**, 191–212.

Gimeno, M.J., Auque, L.F., Acero, P. and Gomez, J.B. (2014) Hydrogeochemical characterization and modeling of groundwater in a potential geological repository for spent nuclear fuel in crystalline rocks (Laxemar, Sweden). *Applied Geochemistry*, **45**, 50–71.

Given, R.K. and Wilkinson, B.H. (1985) Kinetic control of morphology, composition, and mineralogy of abiotic sedimentary carbonates. *Journal of Sedimentary Research*, **55**, 109–119.

Goswami, M., Sengupta, P., Sharma, K., Kumar, R., Shrikhande, V.K., Ferreira, J.M.F. and Kothyial, G.P. (2007) Crystallization behavior of Li_2O–ZnO–SiO_2 glass ceramics system. *Ceramics International*, **33**, 863–867.

Grover, V., Sengupta, P., Bhanumurthy, K., Tyagi, A.K. (2006) Electron Probe Microanalysis (EPMA) investigations in the CeO_2–ThO_2–ZrO_2 system. *Journal of Nuclear Materials*, **350**, 169–172.

Grover, V., Sengupta, P. and Tyagi, A.K. (2007) Sub-solidus phase relations in CeO_2–YSZ and ThO_2–YSZ systems: XRD, high-temperature XRD and EPMA studies. *Materials Science Engineering B*, **138**, 246–250.

Grover, V., Banerji, A., Sengupta, P. and Tyagi, A.K. (2008) Raman, XRD and microscopic investigations on CeO_2–Lu_2O_3 and CeO_2–Sc_2O_3 systems: A sub-solidus phase evolution study. *Journal of Solid State Chemistry*, **181**, 1930–1935.

Grover, V., Cavan, S.V., Sengupta, P. and Tyagi, A.K. (2010) CeO_2–$YO_{1.5}$–$NdO_{1.5}$ system: An extensive phase relation study. *Journal of European Ceramic Society*, **30**, 3137–3143.

Halder, R., Dutta, R.S., Sengupta, P., Samajdar, I. and Dey, G.K. (2014) Microstructural studies on Alloy 693. *Journal of Nuclear Materials*, **453**, 91–97.

Halder, R., Sengupta, P., Sudarsan, V., Ghosh, A., Ghosh, A., Bhukta, A., Sharma, G., Samajdar, I. and Dey, G. K. (2015) Photoluminescence study on irradiated yttria stabilized zirconia. *Journal of Nuclear Materials*, **456**, 359–368.

Hench, L.L., Clark, D.E. and Campbell, J. (1984) High level waste immobilization forms. *Nuclear and Chemical Waste Management*, **5**, 149–173.

Jafar, M., Sengupta, P., Achary, S.N. and Tyagi, A.K. (2014*a*) Structural and phase evolution studies in $CaZrTi_2O_7$ – $Nd_2Ti_2O_7$ systems. *Journal of the American Ceramic Society*, **97**, 609–616.

Jafar, M., Sengupta, P., Achary, S.N. and Tyagi, A.K. (2014*b*) Phase evolution and Microstructural studies in $CaZrTi_2O_7$ (zirconolite)–$Sm_2Ti_2O_7$ (pyrochlore) system. *Journal of the European Ceramic Society*, **34**, 4373–4381.

Kain, V., Sengupta, P., De, P.K. and Banerjee, S. (2005) Case reviews on the effect of microstructure on the corrosion behavior of austenitic alloys for processing and storage of nuclear waste. *Metallurgical Materials Transactions A*, **36A**, 1075–1084.

Kaushik, C.P., Mishra, R.K., Sengupta, P., Das, D., Kale, G.B. and Raj, K. (2006) Barium borosilicate glass: a potential matrix for immobilization of sulfate bearing high level radioactive waste. *Journal of Nuclear Materials*, **358**, 129–138.

Keeney-Kennicutt, W.L. and Morse, J.W. (1984) The interaction of $Np(V)O_2^+$ with common mineral surfaces in dilute aqueous solutions and seawater. *Marine Chemistry*, **15**, 133–150.

Kelly, S.D., Newville, M.G., Cheng, L., Kemner, K.M., Sutton, S.R., Fenter, P., Sturhio, N.C. and Spötl, C. (2003) Uranyl incorporation in natural calcite. *Environmental Science & Technology*, **37**, 1284–1287.

Kelly, S.D., Rasbury, E.T., Chattopadhyay, S., Krof, A.J. and Kemner, K.M. (2006) Evidence of a stable uranyl site in ancient organic-rich calcite. *Environmental Science & Technology*, **40**, 2262–2268.

Kim, C.W. and Day, D.E. (2003) Immobilization of Hanford Law in iron phosphate glasses. *Journal of Non-Crystalline Solids*, **331**, 20–31.

Kitano, Y. and Oomori, T. (1971) The coprecipitation of uranium with calcium carbonate. *Journal of the Oceanographical Society of Japan*, **27**, 34–42.

Kuczumow, A., Genty, D., Chevallier, P., Nowak, J., Florek, M. and Buczynska, A. (2005) X-ray and electron microprobe investigation of the speleothems from Godarville tunnel. *X-ray Spectrometry*, **34**, 502–508.

Kutty, T.R.G., Kulkarni, R.V., Sengupta, P., Khan, K.B., Bhanumurthy, K., Sengupta, A.K., Panakkal, J.P., Kumar Arun and Kamath, H.S. (2008*a*) Development of CAP process for fabrication of ThO_2–UO_2 fuels Part II: Characterization and property evaluation. *Journal of Nuclear Materials*, **373**, 309–318.

Kutty, T.R.G., Nair, M.R., Sengupta, P., Basak, U., Kumar Arun and Kamath, H.S. (2008*b*) Characterization of $(Th\text{-}U)O_2$ fuel pellets made by impregnation technique. *Journal of Nuclear Materials*, **374**, 9–19.

Lee, W.E., Ojovan, M.I. and Stennett, M.C. (2006) Immobilization of radioactive waste in glasses, glass composite. *Advances in Applied Ceramics*, **105**, 3–12.

Mathur, J.N. (1991) Complexation and thermodynamics of the uranyl ion with phosphate. *Polyhedron*, **10**, 47–53.

Mathur, J.N., Murali, M.S., Natarajan, P.R., Badheka, L.P. and Banerji, A. (1992) Extraction of actinides and fission products by octyl(phenyl)-N,N diisobutylcarbamoylmethyl-phosphine oxide from nitric acid media. *Talanta*, **39**, 439–496.

https://doi.org/10.1180/minmag.2016.080.013 Published online by Cambridge University Press

Meece, D.E. and Benninger, J.K. (1993) The coprecipitation of Pu and other radionuclides with $CaCO_3$. *Geochimica Cosmochimica Acta*, **57**, 1447–1458.

Mishra, R.K., Sengupta, P., Kaushik, C.P., Tyagi, A.K., Kale, G.B. and Raj, K. (2007) Studies on immobilization of thorium in barium borosilicate glass. *Journal of Nuclear Materials*, **360**, 143–150.

Mishra, R.K., Sudarsan, V., Sengupta, P., Vatsa, R.K., Tyagi, A.K., Kaushik, C.P., Das, D. and Raj, K. (2008) Role of sulphate in structural modifications of sodium barium borosilicate glasses developed for nuclear waste immobilization. *Journal of American Ceramic Society*, **91**, 3903–3907.

Ojovan, M.I. and Lee, W.E. (2005) *An Introduction to Nuclear Waste Immobilization.* Elseiver, Netherlands, 315 Pp.

Ojovan, M.I. and Lee, W.E. (2007) *New Developments in Glassy Nuclear Wasteforms.* Nova Science Pub Inc, Canada, 131 Pp.

Pirlet, V. (2001) Overview of actinides Np, Pu, Am and Tc release from waste glasses: influence of solution composition. *Journal of Nuclear Materials*, **298**, 47–54.

Quade, J. and Cerling, T.E. (1990) Stable isotopic evidence for a pedogenic origin of carbonates in Trench 14 near Yucca Mountain, Nevada. *Science*, **250**, 1549–1552.

Railsback, L.B., Brook, G.A., Chen, J., Kalin, R. and Fleischer, C.J. (1994) Environmental controls on the petrology of a late Holocene speleothem from Botswana with annual layers of aragonite and calcite. *Journal of Sedimentary Research*, **A64**, 147–155.

Railsback, L.B. (1999) Patterns in the compositions, properties, and geochemistry of carbonate minerals. *Carbonates and Evaporites*, **14**, 1–20.

Ramanujam, A., Achuthan, P.V., Dhami, P.S., Gopalakrishnan, V., Kannan, R. and Mathur, J.N. (1995) Extraction chromatographic separation of promethium from high active waste solutions of purex origin. *Solvent Extraction and Ion Exchange*, **13**, 301–312.

Reeder, R.J., Nugent, M., Lamble, G.M., Tait, C.D. and Morris, D.E. (2000) Uranyl incorporation into calcite and aragonite: XAFS and luminescence studies. *Environmental Science & Technology*, **34**, 638–644.

Reeder, R.J., Nugent, M., Tait, C.D., Morris, D.E., Heald, S.M., Beck, K.M., Hess, W.P. and Lanzirotti, A. (2001) Coprecipitation of uranium(VI) with calcite: XAFS, micro-XAS, and luminescence characterization. *Geochimica et Cosmochimica Acta*, **65**, 3491–3503.

Russell, A.D., Emerson, S., Nelson, B.K., Erez, J. and Lea, D.W. (1994) Uranium in foraminiferal calcite as a recorder of seawater uranium concentrations. *Geochimica et Cosmochimica Acta*, **58**, 671–681.

Ryan, J.L. and Wheelright, E.J. (1959) *The Recovery, Purification, and Concentration of Plutonium by Anion Exchange in Nitric Acid*. Report HW-55893, United States Department of the Environment, Office of Environmental Management. Available from: http://www.osti.gov/scitech/biblio/4232455

Sanwal, J., Kotlia, B.S., Rajendran, C.P., Ahmad, S.M., Rajendran, K. and Sandiford, M. (2013) Climatic variability in Central Indian Himalaya during the last ~1800 years: evidence from a high resolution speleothem record. *Quaternary International*, **304**, 183–192.

Schulz, W.W. and Horwitz, E.P. (1988) The Truex process and the management of liquid TRU waste. *Separation Science and Technology*, **23**, 1191–1210.

Sengupta, P. (2011) Interaction study between nuclear waste glass melt and ceramic melter bellow liner materials. *Journal of Nuclear Materials*, **411**, 181–184.

Sengupta, P. (2012) A review on immobilization of phosphate containing high level nuclear wastes within glass matrix – present status and future challenges. *Journal of Hazardous Materials*, **235–236**, 17–28.

Sengupta, P., Gawde, P.S., Bhanumurthy, K. and Kale, G. B. (2004) Diffusion reaction between Zircaloy 2 and Thoria. *Journal of Nuclear Materials*, **325**, 180–187.

Sengupta, P., Mittra, J. and Kale, G.B. (2006) Interaction between borosilicate melt and Inconel. *Journal of Nuclear Materials*, **350**, 66–73.

Sengupta, P., Kaushik, C.P., Mishra, R.K. and Kale, G.B. (2007) Microstructural characterization and role of glassy layer developed on process pot wall during nuclear high level waste vitrification process. *Journal of the American Ceramic Society*, **90**, 3085–3090.

Sengupta, P., Soudamini, N., Kaushik, C.P., Jagannath, Mishra, R.K., Kale, G.B., Raj, K., Das, D. and Sharma, B.P. (2008) Corrosion of Alloy 690 process pot by sulfate containing high level radioactive waste at feed stage. *Journal of Nuclear Materials*, **374**, 185–91.

Sengupta, P., Kaushik, C.P., Kale, G.B., Das, D., Raj, K. and Sharma, B.P. (2009) Evaluation of Alloy 690 process pot at the contact with borosilicate melt pool during vitrification of high level nuclear waste. *Journal of Nuclear Materials*, **392**, 379–85.

Sengupta, P., Fanara, S. and Chakraborty, S. (2011*a*) Preliminary study on calcium aluminosilicate glass as a potential host matrix for radioactive ^{90}Sr – an approach based on natural analogue study. *Journal of Hazardous Materials*, **190**, 229–39.

Sengupta, P., Rogalla, D., Becker, H.W., Dey, G.K. and Chakraborty, S. (2011*b*) Development of graded Ni-YSZ composite coating on Alloy 690 by pulsed laser deposition technique to reduce hazardous metallic nuclear waste inventory. *Journal of Hazardous Materials*, **192**, 208–21.

https://doi.org/10.1180/minmag.2016.080.013 Published online by Cambridge University Press

Sengupta, P., Kaushik, C.P. and Dey, G.K. (2013) Immobilization of high-level nuclear wastes: The Indian Scenario. Pp. 25–51 in: *On a Sustainable Future of the Earth's Natural Resources* (M. Ramkumar, editor). Springer-Verlag.

Sengupta, P., Dey, K.K., Halder, R., Ajithkumar, T.G., Abraham, G., Mishra, R.K., Kaushik, C.P. and Dey, G.K. (2014) Vanadium in borosilicate glasses. *Journal of the American Ceramic Society*, DOI: 10.1111/jace.13303

Serrano, M.J.G., Salazar, P.A., Sanz, L.F.A. and Jimenez, Y. J.B.G. (2008) Fracture sealing by mineral precipitation in a Deep Geological Nuclear Waste Repository. *Revista de la Sociedad Espanola de Mineralogia*, **9**, 119–120.

Shanbhag, P.M. and Morse, J.W. (1982) Americium interaction with calcite and aragonite surfaces in seawater. *Geochimica et Cosmochimica Acta*, **46**, 241–246.

Sharma, B.I., Goswami, M., Sengupta, P., Shrikhande, V. K., Kale, G.B. and Kothiyal, G.P. (2004) Study on some thermo physical properties in Li_2O–ZnO–SiO_2 glass ceramics. *Materials Letters*, **58**, 2423–2428.

Sposito, G.A. (1986) Distinguishing adsorption from surface precipitation. Pp. 217–228 in: *Geochemical Processes at Mineral Surfaces* (J.A. Davis and K.H. Hayes, editors). Symposium Series 323. American Chemical Society, Washington, DC.

Stumpf, T. and Fanghänel, T. (2002) A Time-Resolved Laser Fluorescence Spectroscopy (TRLFS) Study of the interaction of trivalent actinides (Cm(III)) with calcite. *Journal of Colloid and Interface Science*, **249**, 119–122.

Sturchio, N.C., Antonio, M.R., Soderholm, L., Sutton, S. R. and Brannon, J.C. (1998) Tetravalent uranium in calcite. *Science*, **281**, 971–973.

van Cappellen, P., Charlet, L., Stumm, W. and Wersin, P. (1993) A surface complexation model of the carbonate mineral-aqueous solution interface. *Geochimica et Cosmochimica Acta*, **57**, 3505–3518.

Webster, J.W., Brook, G.A., Railsback, L.B., Cheng, H., Edwards, R.L., Alexander, C. and Reeder, P.P. (2007) Stalagmite evidence from Belize indicating significant droughts at the time of preclassic abandonment, the Maya Hiatus, and the classic Maya collapse. *Palaeogeography Palaeoclimate Palaeoecology*, **250**, 1–17.

White, W.B. (1997) Thermodynamic equilibrium, kinetics, activation barriers, and reaction mechanisms for chemical reactions in Karst terrains. *Environmental Geology*, **30**, 46–58.

Zachara, J.M., Cowan, C.E. and Resch, C.T. (1991) Sorption of divalent metals on calcite. *Geochimica Cosmochimica Acta*, **55**, 1549–1562.

Zavarin, M., Roberts, S.K., Hakem, N., Sawvel A.M. and Kersting, A.B. (2005) Eu(III), Sm(III), Np(V), Pu(V), and Pu(IV) sorption to calcite. *Radiochimica Acta*, **93**, 93–102.